

1 **The Unexpected Oceanic Peak in Energy Input to the**
2 **Atmosphere and its Consequences for Monsoon**
3 **Rainfall**

4 **Nandini Ramesh^{1,2}, William R. Boos^{2,3}**

5 ¹ARC Centre for Data Analytics for Resources and the Environment, University of Sydney, 1 Cleveland

6 Street, Darlington 2008, NSW, Australia. (Current affiliation)

7 ²Department of Earth and Planetary Science, University of California, Berkeley, McCone Hall, Berkeley,

8 California, 94720

9 ³Climate and Ecosystem Sciences Division, Lawrence Berkeley National Laboratory, 1 Cyclotron Road,

10 Berkeley, CA 94720

11 **Key Points:**

- 12 • The maximum energy input to the atmosphere in boreal summer lies over the north-
13 ern Indian Ocean
- 14 • Cloud radiative effects strongly enhance energy input over ocean compared to land
- 15 • Surface heat capacity contrasts interact with cloud radiative effects to shift mon-
16 soon rainfall

Abstract

Monsoons have historically been understood to be caused by the low thermal inertia of land, allowing more energy from summer insolation to be transferred to the overlying atmosphere than over adjacent ocean. Here we show that during boreal summer, the global maximum net energy input (NEI) to the atmosphere unexpectedly lies over the Indian Ocean, not over land. Observed radiative fluxes suggest that cloud-radiative effects (CRE) almost double the NEI over ocean, shifting the NEI peak from land to ocean. Global climate model experiments with both land and interactive sea surface temperatures confirm that CRE create the oceanic NEI maximum. Interactions between CRE, NEI, circulation, and land-sea contrast in surface heat capacity shift precipitation from Southeast to South Asia. CRE thus alter the global partitioning of precipitation between land and ocean and the spatial structure of Earth's strongest monsoon, in ways that can be understood through the NEI.

Plain Language Summary

Land's influence on the energy supplied to the atmosphere has long been recognized as a leading cause of monsoons. From early theories conceptualizing monsoons as continental-scale sea breezes responding to land-sea temperature contrasts, to modern frameworks based on air's total energy content, the energy input to the atmosphere over land has been assumed higher than that over ocean in the summer hemisphere. We show that, instead, in the Asian region, the energy input to the atmosphere is larger over ocean than land because of clouds' effects on radiation. Observations and simulations indicate that the spatial pattern of tropical rainfall is set by interactions between clouds and the land-sea contrast in surface heat capacity, mediated by atmospheric circulation.

1 Introduction

Monsoons have, for over a century, been known to be caused by land-sea contrast (Blanford, 1888; Ananthakrishnan et al., 1965). The low thermal inertia of off-equatorial land allows more energy from summer insolation to be transferred to the overlying atmosphere there than over the near-equatorial ocean; this sets up a thermally direct circulation with precipitating ascent over the continent. This precipitating circulation was traditionally seen as a continental-scale sea breeze responding to land-sea temperature contrast, but in recent decades has been better understood by including the latent heat of water vapor in measures of energy, such as the widely used moist static energy (MSE). A general understanding of controls on the structure of monsoons was obtained using a series of idealized climate models in which air's MSE is a central variable (Chou et al., 2001; Neelin, 2007; Plumb, 2007).

As an alternative to theoretical frameworks based on the energy content of air, frameworks based on energy sources, i.e., the net energy input (NEI) to the atmosphere, have been explored (Biasutti et al., 2018). The NEI is the sum of surface turbulent fluxes (sensible and latent heat) and the net radiative flux into the atmospheric column; horizontal contrasts in NEI can be viewed as a forcing for tropical circulations, which are typically "energetically direct" with an ascent branch near the NEI and MSE maxima. Radiative and wind-evaporation feedbacks can render the NEI diagnostic, rather than a true exogenous forcing, but these feedbacks often exhibit substantial cancellation (Peterson & Boos, 2020; Lagu   et al., 2021). The seasonal cycle of tropical precipitation maxima is strongly associated with that in NEI and, through conservation of energy, with zonal and meridional energy fluxes carried by time-mean overturning tropical atmospheric circulations (Kang et al., 2008; Donohoe et al., 2013; Boos & Korty, 2016; Adam et al., 2016).

Despite this theoretical focus on NEI as a driver of tropical circulations, few studies have examined observationally-based estimates of NEI, especially with the goal of un-

derstanding how observed spatial structures influence regional precipitation. Top-of-atmosphere (TOA) radiative fluxes have been used to show that there is positive NEI over continents in the summer hemisphere, with weaker values over ocean and strong negative NEI over continents in the winter hemisphere (Chou & Neelin, 2003); such studies argued that an energetically direct circulation results, with precipitating ascent over summer continents. A review of the dynamics of tropical convection zones and monsoons (Neelin, 2007) stated that NEI was systematically larger over land than ocean by $50\text{-}100 \text{ W m}^{-2}$, with that contrast driving planetary-scale monsoon flow. Here we highlight a surprising deviation from this view of land-ocean contrast: an oceanic maximum in NEI that we show strongly influences the spatial structure of precipitation in Asia. We build on prior studies of cloud radiative effects (CRE) in monsoons (Sharma, 1998; Rajeevan & Srinivasan, 2000; J. Li et al., 2017) to show that CRE play a key role in setting this spatial pattern of NEI (Section 4). Using a general circulation model (GCM) that, unlike in prior studies of the influence of CRE on precipitation (Voigt & Albern, 2019; Byrne & Zanna, 2020), accounts for the differing thermal inertia between ocean and land, we show that differences in the response of the land and sea surface to CRE establish this oceanic NEI maximum and set the structure of precipitation (Section 5).

2 Materials and Methods

This study uses atmospheric reanalyses, observations, and a global climate model. All data used here are publicly available. Figures 1-2 use the European Centre for Medium-Range Weather Forecasts (ECMWF) Reanalysis Version 5 (ERA5) (Hersbach et al., 2020) (1979-2018) so as to display an internally-consistent estimate of NEI and its components. Findings reported here were verified against other reanalyses and observational products, listed below. Conclusions were based only on features for which all listed datasets displayed qualitative agreement.

2.1 Reanalysis Products

In addition to ERA5, we use surface turbulent and radiative fluxes and TOA radiative fluxes from these reanalyses in Figure 1(c):

1. The National Center for Environmental Prediction Climate Forecast System Reanalysis, Version 2 (**CFSR**)(Saha et al., 2014) (1979-2016)
2. The ECMWF Interim Reanalysis (**ERA-I**)(Dee et al., 2011) (1979-2015)
3. The Japanese Meteorological Agency 55-year Reanalysis (**JRA**)(Kobayashi et al., 2015) (1979-2008)
4. The National Aeronautics and Space Administration (NASA) Modern-Era Retrospective Analysis for Research and Applications, version 2 (**MERRA2**)(Gelaro et al., 2017) (1980-2015)
5. The National Center for Environmental Prediction-Department of Energy Reanalysis II (**NCEP**)(Kanamitsu et al., 2002) (1948-2018)

2.2 Observational Products

We also use the following observational estimates of ocean surface fluxes, surface and TOA radiative fluxes, cloud fraction, and precipitation:

2.2.1 Air-Sea Turbulent Fluxes

1. The National Oceanography Centre Surface Flux and Meteorological Dataset (**NOCS**)(Berry & Kent, 2009) (2000-2018)
2. The Woods Hole Oceanographic Institution Objectively-Analyzed Air-Sea Flux Project, version 3 (**OAFlux**)(Yu & Weller, 2007) (1958-2018)

- 112 3. The National Oceanic and Atmospheric Administration (NOAA) Climate Data
 113 Record of Ocean Heat Fluxes, version 2 (**SeaFlux**) (Clayson et al., 2016) (2000-
 114 2020)

115 **2.2.2 Radiative Fluxes**

116 Clouds and the Earth's Radiant Energy System Energy Balanced and Filled TOA
 117 edition-4.0 data product (**CERES**) (Loeb et al., 2018). In figures where this is combined
 118 with other datasets, the overlapping years of 2000-2018 are used.

119 **2.2.3 Cloud Fraction**

120 The Cloud-Aerosol Lidar and Infrared Pathfinder Satellite Observations (CALIPSO)
 121 General Circulation Model (GCM)-Oriented Cloud CALIPSO Product (**CALIPSO-GOCCP**) (Chepfer
 122 et al., 2010) (2001-2018). In Figure S2, we use CALIPSO-GOCCP's definition of high
 123 clouds, i.e., clouds above 6.5 km altitude, to calculate high cloud fraction. High cloud
 124 fraction is computed as the maximum cloud area fraction over all layers higher than this
 125 threshold.

126 **2.2.4 Precipitation**

127 The Global Precipitation Climatology Project (**GPCP**) version 2.3 (Adler et al.,
 128 2018). A climatology was calculated using monthly means from 1979 to 2020.

129 **2.3 Estimation of Net Energy Input**

130 We estimate the net energy input (NEI) as the sum of upward surface turbulent
 131 fluxes, upward surface radiative fluxes, and downward top-of-atmosphere (TOA) radia-
 132 tive fluxes. All terms needed to calculate this quantity are included in the reanalyses.

133 In observational products, we use TOA and surface radiative fluxes from CERES
 134 with turbulent surface fluxes over ocean from each of the observational products listed.
 135 It is difficult to obtain estimates of the global distribution of surface turbulent fluxes over
 136 land; however, due to the low heat capacity of land, the net land surface energy flux is
 137 near zero on seasonal timescales and therefore the NEI is nearly equal to the TOA flux
 138 over land (Neelin, 2007). In some regions, a small amount of energy (generally not ex-
 139 ceeding 20 W m^{-2}) is consumed at the surface through processes such as seasonal snowmelt;
 140 we account for this by computing the difference between NEI and TOA flux over land
 141 from ERA5 and applying this as a correction to arrive at the NEI over land in Figure 1(c).

142 **2.4 Global Climate Model Experiments**

143 We use the Community Earth System Model (CESM) version 2.0, with the scientifically-
 144 validated "ETEST" component set. This consists of a global atmosphere model at a res-
 145 olution of $2.5^\circ \times 1.875^\circ$ with 32 vertical levels, coupled to a slab ocean 30 m deep, using
 146 a climatological q-flux (i.e., a spatially-varying heat flux in the ocean representing the
 147 effects of ocean heat transport and processes such as ice melt/freezing) derived from a
 148 coupled control run of the model. In this component set, the Community Land Model
 149 (CLM5.0) is used with satellite phenology, and greenhouse gas concentrations are held
 150 at pre-industrial (year 1850) levels. A 5-year spinup was used before the experiments were
 151 performed.

152 Because we focus on the impacts of cloud-radiative effects during boreal summer,
 153 we initiate all experiments from May 1st of the 6th year of a control run. This prevents
 154 model drift due to the altered conditions in the experiments from affecting the season
 155 of interest. The "noTropicCloud" experiment consists of an ensemble of five simulations

156 in which radiative effects of clouds within the latitudes 35°S-35°N were set to zero, i.e.,
 157 clouds within the tropical belt were transparent to both shortwave and longwave radia-
 158 tion. This is similar to the method used in the Clouds On-Off Climate Intercompar-
 159 ision Experiment (COOKIE)(Stevens et al., 2012), except using prognostic instead of pre-
 160 scribed SST. The latitude of 35° was chosen as it corresponds to the latitude where the
 161 annual-mean, zonal-mean TOA fluxes change sign. Each of the five simulations was ini-
 162 tiated with a different small perturbation.

163 The control experiment consists of a similarly-designed ensemble, with CRE ac-
 164 tive. Results presented are averaged over these ensembles. In figures where differences
 165 between the control and noTropicCloud are shown, only areas where differences were sig-
 166 nificant at the 95% level based on a two-tailed t-test are shaded.

167 3 The Observed Distribution of Net Energy Input

168 During local summer in each hemisphere, NEI is typically largest over land (Fig-
 169 ure 1(a, b)), acting as an energy source for the circulation. This pattern is consistent with
 170 the view that monsoon circulations are driven by a continental energy source maximum (Neelin,
 171 2007). For South Asia, however, the atmosphere gains substantially more energy over
 172 the Bay of Bengal than over adjacent land, which is, according to several datasets, the
 173 global maximum of NEI in boreal summer. Despite wide variation in the estimated NEI
 174 across reanalyses and observational products (Figure 1(c)), all display an NEI peak over
 175 the Northern Indian Ocean.

176 We decompose the NEI into surface and TOA components, showing that the net
 177 surface energy flux (including radiation) is near zero or negative over the Bay of Ben-
 178 gal and Arabian Sea during boreal summer, despite the large surface turbulent heat fluxes
 179 into the atmosphere there (Figure 2(a), Figure S1). Over the Northern Indian Ocean,
 180 TOA fluxes contribute most of the positive NEI (Figure 2(b)), suggesting a role played
 181 by processes that influence TOA radiation, such as clouds. The shortwave and longwave
 182 components of the CRE (Figure 2(c)) confirm this: while the shortwave effect of clouds
 183 reflects energy into space and is therefore negative over the region experiencing monsoon
 184 rainfall, the longwave effect, which retains energy in the atmospheric column, is largest
 185 over the Bay of Bengal NEI maximum. This reduction in energy loss to space coincides
 186 with an area covered by high cloud tops (Figure S2); the frequent occurrence of orga-
 187 nized mesoscale convective systems in this region likely contributes to this large high-
 188 cloud fraction (P.-J. Chen et al., 2021; Hamada et al., 2014; Yuan & Houze, 2010; Luo
 189 et al., 2017). The resulting net CRE (Figure 2(d)) thus makes a large positive contri-
 190 bution to the NEI over the northern Indian Ocean.

191 4 The Prognostic Influence of Cloud Radiative Effects

192 While observed radiative fluxes can be used to estimate the net influence of clouds
 193 on radiation given the observed atmospheric state (e.g. Figure 2(d)), it is possible that
 194 large changes in wind, temperature, humidity, and cloud properties would occur in the
 195 absence of CRE. This motivates our use of the climate model described in Section 2 to
 196 determine, prognostically, the influence of CRE on both the NEI and the large-scale cir-
 197 culation.

198 The control run captures key features of the NEI distribution, including the energy
 199 sources over ocean in the Southern Hemisphere and Northern Hemisphere continents,
 200 and the maximum over the northern Indian Ocean during boreal summer (Figure 3(a)).
 201 There is some bias relative to ERA5, but this is of comparable magnitude to the obser-
 202 vational uncertainty in NEI (e.g. Fig. 1(c)). The CRE contribution to NEI (Figure 3(b)),
 203 calculated as the difference between clear-sky and all-sky radiative effects, in the con-
 204 trol run is similar to that in observations (Figure 2(d)).

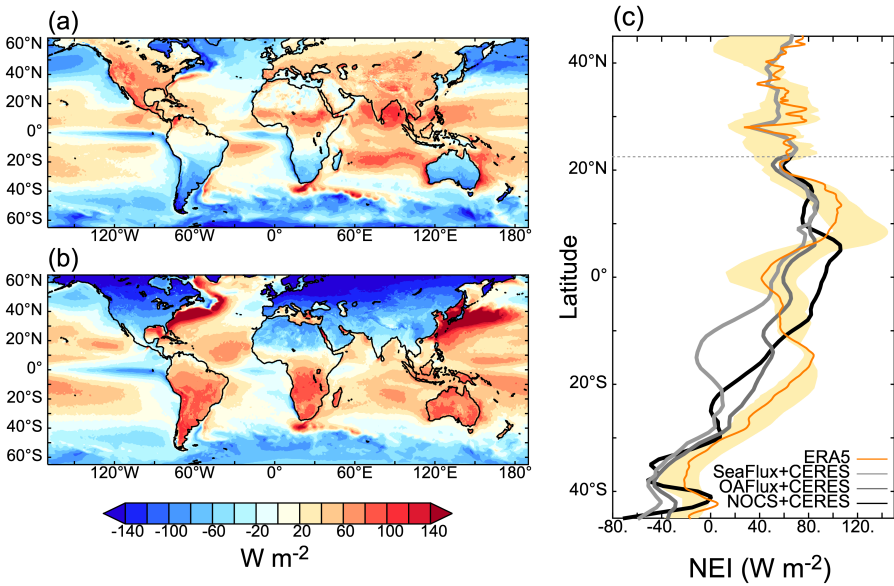


Figure 1. The oceanic nature of the energy input maximum during boreal summer: The climatological net energy input (W/m^2) to the atmospheric column in (a) boreal summer (June-August) and (b) austral summer (December-February) from ERA5. (c) Net energy input into the atmosphere from three observational estimates (thick grey lines) and ERA5 (orange line) averaged over the longitudes of the Bay of Bengal (90°E - 95°E) in boreal summer. The filled area indicates the range of the same quantity from five other reanalysis products (listed in Section 2.1). The dotted line indicates the latitude of the northern edge of the Bay of Bengal.

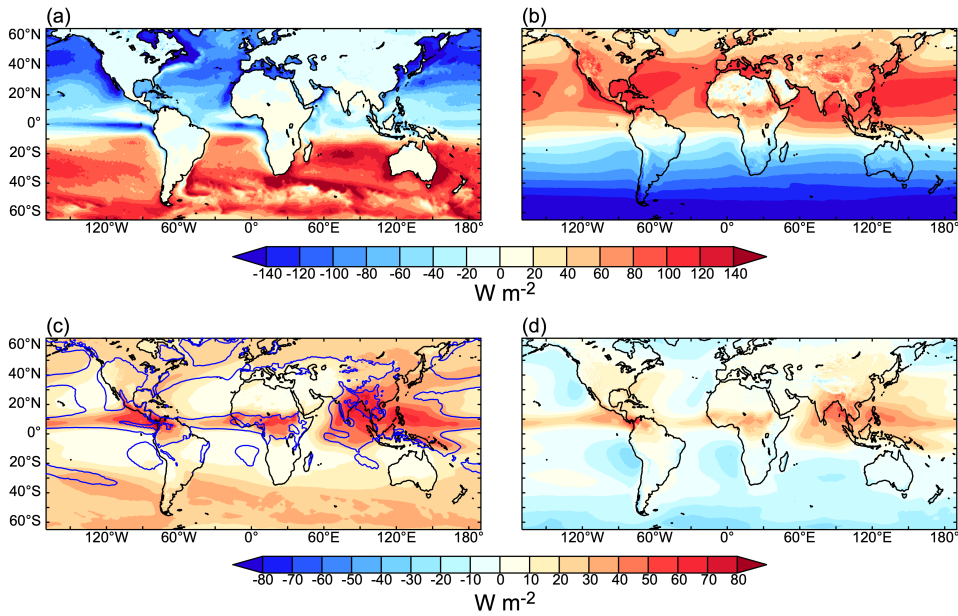


Figure 2. Components of the observed energy input: The contributions of fluxes at (a) the surface and (b) the top of the atmosphere to the climatological NEI. Panel (c) shows the contributions of the longwave (colors) and shortwave (contours; intervals of -50 W m^{-2}) components of CRE respectively. The total estimated contribution of CRE is shown in (d). Quantities are positive if they contribute to the energy content of the atmospheric column.

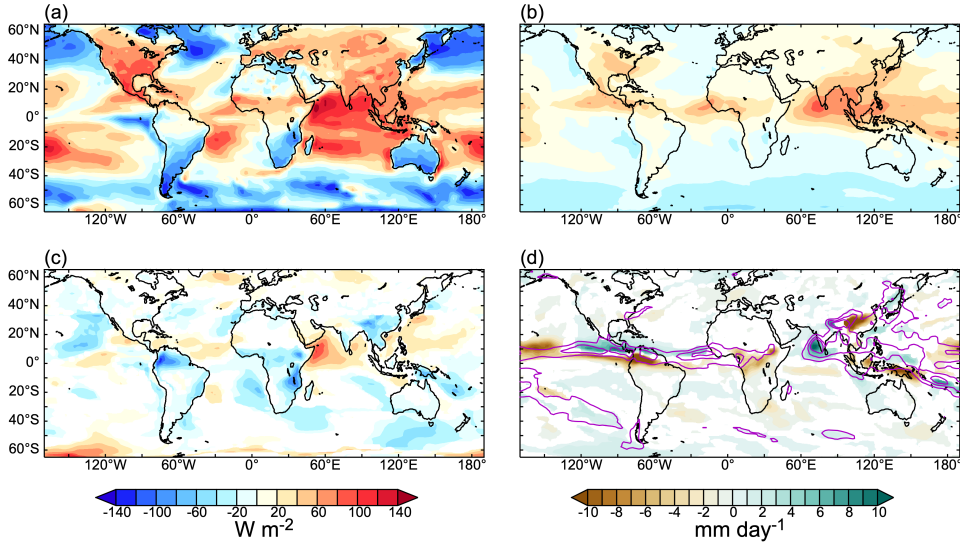


Figure 3. Perturbing cloud-radiative effects in a global model: The June–August mean (a) NEI, and (b) CRE contribution to NEI from the control ensemble, calculated as the difference between all-sky and clear-sky radiative effects. The bottom row shows the June–August mean contribution of CRE inferred prognostically (control minus noTropicCloud) (c) to NEI and (d) to precipitation. Contours in (d) indicate the June–August mean precipitation in the control ensemble at 5-mm/day increments.

Examining the difference between the control run and the run with CRE eliminated in the tropics (the noTropicCloud experiment), confirms that clouds enhance NEI over the entire Northern Indian Ocean (Figure 3(c)). However, tropical CRE also reduces NEI over several land areas, particularly Southeast Asia. Overall, the response to removing clouds in the model experiment differs greatly from the CRE inferred simply as the difference between all-sky and clear-sky radiative effects (Figure 3(b)), indicating that CRE induces feedbacks on surface turbulent fluxes and radiation.

The absence of CRE substantially alters boreal summer precipitation (Figure 3(d)). Notably, including CRE reduces rainfall over tropical land relative to that over ocean. The fraction of total summer rainfall within the latitude range of eliminated CRE (35°S–35°N) that occurs over land increases from 0.2 in the control to 0.25 in the noTropicCloud experiment (a relative increase of 26% ($\pm 4\%$, one standard deviation)); in the deep tropics (20°S–20°N), this re-partitioning of rainfall over land versus ocean is even more pronounced, with a relative increase of 31% ($\pm 7\%$).

The spatial pattern of changes to rainfall is dominated by shifts in precipitation maxima. Over the Atlantic and East Pacific, the oceanic ITCZ is displaced to the north when CRE are included. This is consistent with previous aquaplanet studies (Voigt et al., 2014) that concluded that CRE shift the ITCZ poleward by producing interhemispheric NEI asymmetries. Over the Indo-Pacific, however, the spatial pattern of changes in precipitation is more complex, displaying a striking southwestward shift of rainfall from East Asia to South Asia when CRE is added.

226 **5 The Influence of Cloud Radiative Effects on Atmospheric Circula-**
 227 **tion**

228 The cause of this mostly zonal shift over Asia can be understood using dynamic
 229 or energetic perspectives. We first describe how CRE alter the distributions of precip-
 230 itation, surface enthalpy fluxes, and MSE advection, then use an energetic framework
 231 to show how the influence of clouds on NEI is quantitatively consistent with the model-
 232 simulated precipitation shift.

233 We treat the noTropicCloud experiment as a basic state on which CRE can be ap-
 234 plied. In that state, boreal summer precipitation peaks over southeastern Asia (Figure 4(a),
 235 gray contours), consistent with idealized model simulations that show monsoon precip-
 236 itation concentrates over the eastern part of rectangular tropical continents due to the
 237 Rossby gyres that comprise three-dimensional monsoon circulations (Chou et al., 2001;
 238 Privé & Plumb, 2007; S.-P. Xie et al., 1999). In those studies, much of this concentra-
 239 tion of rainfall over the eastern part of the continent is due to advection of dry air by
 240 the lower-tropospheric Rossby gyre. We see evidence for that in the noTropicCloud run:
 241 the strong zonal MSE gradient over South Asia (Figure 4(a)) is spanned by low-level east-
 242 ward winds that feed into the region of peak precipitating ascent (Figure 4(b)), as ex-
 243 pected for the linear Rossby gyre component of a monsoon (Gill, 1980; Hoskins & Rod-
 244 well, 1995). The resulting advection of MSE, vertically integrated over the atmosphere,
 245 provides a negative energy tendency over much of South and Southwest Asia exceeding
 246 150 W m^{-2} (Figure 4(b)). Horizontal advection by the Rossby gyre thus greatly com-
 247 pensates the radiative forcing for precipitation over South Asia in the absence of CRE.
 248

249 With tropical CRE turned on, the shortwave effects of clouds over southeastern Asia
 250 reduce surface enthalpy fluxes there by about 100 W m^{-2} (Figure 4(c)). Although the
 251 longwave effects warm the atmosphere by $30\text{--}50 \text{ W m}^{-2}$, opposing the shortwave con-
 252 tribution to the NEI, the net CRE is negative, weakening the thermally-forced Rossby
 253 gyre. CRE also convectively stabilize the troposphere, as evidenced by the upper-tropospheric
 254 warming and lower-tropospheric cooling seen in the response to tropical CRE (Figure S3).
 255 This convective stabilization over land leads to a reduction in precipitating ascent over
 256 Southeast Asia (Figure 4(e)), a weakening of the low-level eastward inflow to that re-
 257 gion, and a reduction in the negative MSE advection over northern India accomplished
 258 by that inflow (Figure 4(d)). This reduction in negative MSE advection peaks around
 259 200 W m^{-2} , and is accompanied by enhanced low-level MSE over South Asia and in-
 260 creased precipitation there (Figure 4(f)); note the MSE increase over Southeast Asia peaks
 261 in the mid-troposphere, consistent with its modification by free-tropospheric CRE rather
 262 than low-level moisture advection. In summary, CRE convectively stabilizes the conti-
 263 nental precipitation maximum and weakens the associated Rossby gyre, reducing the dry
 264 air advection that would otherwise suppress precipitating ascent over South Asia (Fig-
 265 ure 4(e)).

266 One can alternatively view this process in terms of the influence of CRE on NEI
 267 over land, which is negative because the shortwave part of CRE exceeds the longwave
 268 part there. A negative NEI anomaly is thus induced over Southeast Asia by CRE, and
 269 this must be balanced by an anomalous flux of energy into the region, which in the trop-
 270 ics is typically accomplished by time-mean overturning circulations (Kang et al., 2008;
 271 Boos & Korty, 2016). Figure 4(g) shows the energy flux prime meridian (EFPM) in the
 272 control and noTropicCloud experiment, with the EFPM being the zero line of the diver-
 273 gent eastward energy flux (vertically integrated over the atmosphere); the EFPM is ex-
 274 pected to move together with zonal shifts in zonal overturning circulations (Boos & Ko-
 275 rty, 2016), similar to the way the energy flux equator (EFE) moves with meridional shifts
 276 in meridional overturning circulations (Kang et al., 2008). The inclusion of CRE, by al-
 277 tering the spatial pattern of NEI, shifts the EFPM westward by 5.8° , closely matching
 278 the location of the EFPM in reanalyses over the Bay of Bengal (Boos & Korty, 2016).

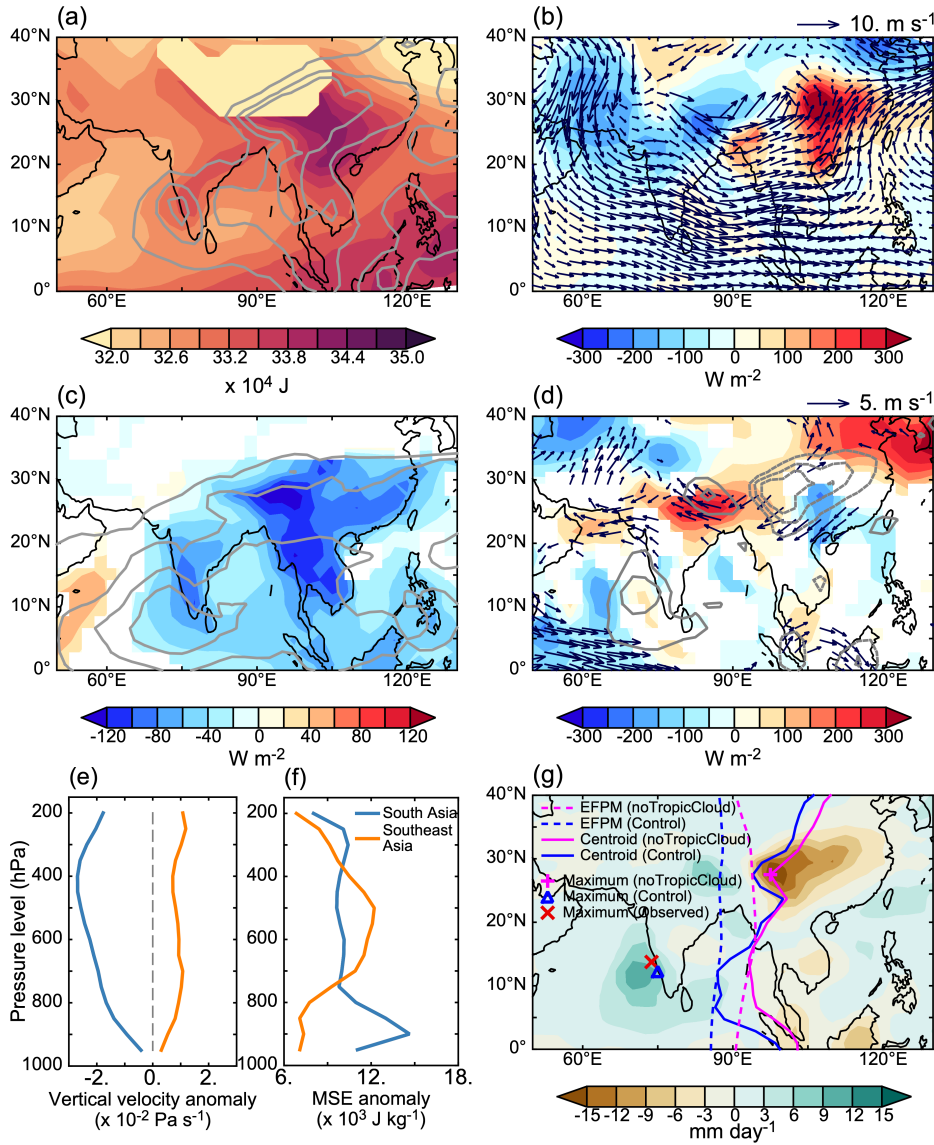


Figure 4. CRE induce a westward shift and weakening of the precipitating Rossby gyre over Asia: (a) Precipitation (grey contours, interval 5 mm day⁻¹) and MSE at 700 hPa (shading) in the noTropicCloud experiment. (b) Vertically-integrated MSE advection in the absence of CRE (shading) with wind velocity (arrows) at 700 hPa. (c) The anomaly (control minus NoTropicCloud) in surface turbulent fluxes (shading, W m⁻²) and column-integrated radiative flux convergence (grey contours, interval 20 W m⁻², negative contours dashed and zero contour omitted). (d) Anomaly (control minus NoTropicCloud) in the quantities shown in (b) and precipitation (grey contours, interval 5 mm day⁻¹, negative contours dashed and zero contour omitted). (e) and (f) show the anomaly (control minus noTropicCloud) in vertical velocity and MSE, respectively, averaged over South (70°E-90°E, 10°N-30°N) and Southeast (90°E-110°E, 10°N-30°N) Asia. (g) Anomaly (control minus noTropicCloud) in precipitation (shading) with the EFPM (dashed lines) and precipitation centroid (solid lines). Symbols indicate the location of maximum seasonal-mean precipitation.

279 A corresponding westward shift in precipitation occurs, with the precipitation centroid
 280 moving 4.3° westward in the meridional mean over the region shown. This constitutes good
 281 agreement, as shifts in the zero lines of divergent energy flux are typically highly cor-
 282 related with but larger than the shifts in precipitation maxima (Kang et al., 2008; Shekhar
 283 & Boos, 2016). Including CRE also shifts the precipitation maximum from continental
 284 Southeast Asia to its observed location over ocean (Figure 4(g)).

285 6 Discussion

286 Our analysis of the observed NEI distribution revealed that in boreal summer, the
 287 global maximum NEI is positioned over the northern Indian Ocean rather than over land,
 288 challenging the conventional view that large-scale tropical circulations in solstice seasons
 289 are associated with continental NEI maxima. When the NEI was decomposed, CRE were
 290 found to be the primary contributor to this maximum. This is distinct from other ob-
 291 served NEI maxima over oceans, where turbulent surface fluxes dominate (e.g., the west-
 292 ern boundary currents and trade wind regions in the winter hemisphere; Figure 1(a,b)).

293 Prior studies have examined the distribution of CRE in monsoons, showing, e.g.,
 294 that the observed net CRE in the Asian monsoon is negative (Rajeevan & Srinivasan,
 295 2000), and that net CRE over Asia is more negative for higher-altitude cloud tops (Saud
 296 et al., 2016). In simulations with realistic boundary conditions, CRE have been shown
 297 to amplify natural modes of Asian monsoon variability (Lu et al., 2021). Previous aqua-
 298 planet studies identified meridional shifts of precipitation maxima in response to CRE
 299 (Voigt et al., 2014; Randall et al., 1989; Byrne & Zanna, 2020; Harrop & Hartmann, 2016;
 300 Popp & Silvers, 2017); in contrast, we found that with realistic continents, the primary
 301 response to CRE over Asia is instead a zonal shift. This zonal shift is produced by the
 302 contrasting effects of CRE over land and ocean combined with the three-dimensional large-
 303 scale tropical circulation. Over land, low surface heat capacity allows the shortwave ef-
 304 fect of clouds to cool the surface and convectively stabilize the atmosphere; over ocean,
 305 shortwave CRE has a weaker effect due to the ocean's high heat capacity. This means
 306 that over ocean, longwave CRE is the dominant contributor to the NEI, warming the
 307 atmosphere (Randall et al., 1989) even though shortwave and longwave CRE approx-
 308 imately cancel at TOA (Tian & Ramanathan, 2002).

309 The asymmetry in CRE between ocean and land is reflected in the large increase
 310 in the proportion of rainfall occurring over land when CRE is eliminated (a relative in-
 311 crease of 26%) and the inland shift of the location of maximum precipitation (Figure 4(g)).
 312 When the NEI and convective instability are reduced in the region of the precipitation
 313 maximum, the Rossby gyre circulation weakens, allowing precipitation to shift westward.
 314 This reduction in convective activity over land is consistent with theoretical models show-
 315 ing that CRE provides a negative feedback on the response to forcings over land (Zeng
 316 & Neelin, 1999), in contrast with the positive feedback on circulations that CRE can pro-
 317 vide over ocean (Su & Neelin, 2002). The dry and wet biases in CESM and many other
 318 climate models over continental South (Sperber et al., 2013; S. Xie et al., 2012) and South-
 319 east Asia (Ma et al., 2014; W.-T. Chen et al., 2019), respectively, suggest that the true
 320 magnitude of this response may be larger than that seen in our experiments.

321 Our findings prompt a rethinking of the role of land-sea contrast in setting the dis-
 322 tribution of tropical NEI: in the largest monsoon system, the NEI maximum lies over
 323 ocean instead of land. Our findings also highlight the importance of differences between
 324 the land and ocean response to CRE. While CRE have long been recognized as a cru-
 325 cial process in atmospheric circulation (Randall et al., 1989; Tian & Ramanathan, 2002;
 326 Sherwood et al., 1994; Sohn & Smith, 1992; Slingo & Slingo, 1988; Y. Li et al., 2015) and
 327 a key determinant of its response to increasing greenhouse gas concentrations (Hansen
 328 et al., 1984; Voigt & Shaw, 2015; Voigt & Albern, 2019; Cepi & Hartmann, 2016; Cepi
 329 et al., 2017), they have frequently been studied in aquaplanets (Voigt et al., 2014; Ran-

330 dall et al., 1989; Byrne & Zanna, 2020; Harrop & Hartmann, 2016; Voigt & Shaw, 2015;
 331 Ceppi & Hartmann, 2016) or settings where the ocean's heat capacity is unaccounted
 332 for (Sherwood et al., 1994; Slingo & Slingo, 1988; Y. Li et al., 2015; Hansen et al., 1984).
 333 The results of this study suggest that the way forward in understanding the impacts of
 334 CRE on atmospheric circulation and patterns of precipitation must necessarily include
 335 the effects of spatial contrasts in the heat capacity of the underlying surface.

336 Acknowledgments

337 N.R. was partially supported by the Australian Research Council (Data Analytics
 338 for Resources and Environments, Grant IC190100031) during the completion of this
 339 work. This material is based on work supported by the U.S. Department of Energy (DOE),
 340 Office of Science, Office of Biological and Environmental Research, Climate and Envi-
 341 ronmental Sciences Division, Regional and Global Model Analysis Program, under Award
 342 DE-SC0019367. It used resources of the National Energy Research Scientific Comput-
 343 ing Center (NERSC), which is a DOE Office of Science User Facility.

344 Open Research and Data Availability Statement

345 All observational and reanalysis data used in this study are publicly available from
 346 the sources listed below:

- 347 • ERA5 (Hersbach et al., 2020): <https://confluence.ecmwf.int/display/CKB/How+to+download+ERA5>
- 348 • CFSR (Saha et al., 2014): <https://www.ncei.noaa.gov/access/metadata/landing-page/bin/iso?id=gov.noaa.ncdc:C00765>
- 349 • JRA (Kobayashi et al., 2015): https://jra.kishou.go.jp/JRA-55/index_en.html
- 350 • MERRA2 (Gelaro et al., 2017): <https://disc.gsfc.nasa.gov/datasets?sort=-timeRes&project=MERRA-2>
- 351 • NCEP (Kanamitsu et al., 2002): <https://psl.noaa.gov/data/gridded/data.ncep.reanalysis2.html>
- 352 • NOCS (Berry & Kent, 2009): <https://noc.ac.uk/science/sustained-observations/noc-surface-flux-dataset>
- 353 • OAFlux (Yu & Weller, 2007): http://apdrc.soest.hawaii.edu/datadoc/whoi_oafluxmon.php
- 354 • SeaFlux (Clayson et al., 2016): <https://seafux.org/data-2/data>
- 355 • CERES (Loeb et al., 2018): <https://ceres.larc.nasa.gov/data/>
- 356 • CALIPSO-GOCCP (Chepfer et al., 2010): <https://climserv.ipsl.polytechnique.fr/cfmiobs/>
- 357 • GPCP (Adler et al., 2018): http://eagle1.umd.edu/GPCP_ICDR/

365 The output of the described climate model experiments, along with instructions to re-
 366 produce the experiments, are available in a Zenodo repository
 367 (DOI:10.5281/zenodo.5704060).

368 References

- 369 Adam, O., Bischoff, T., & Schneider, T. (2016). Seasonal and interannual varia-
 370 tions of the energy flux equator and itcz. part i: Zonally averaged itcz position.
 371 *Journal of Climate*, 29(9), 3219–3230.
- 372 Adler, R. F., Sapiano, M. R., Huffman, G. J., Wang, J.-J., Gu, G., Bolvin, D., ...
 373 others (2018). The global precipitation climatology project (gpcp) monthly
 374 analysis (new version 2.3) and a review of 2017 global precipitation. *Atmo-*
 375 *sphere*, 9(4), 138.

- 376 Ananthkrishnan, R., Ramakrishnan, A., Selvam, M. M., & Rajagopalachari, P.
 377 (1965). Seasonal variations in the zonal and meridional circulation over india.
 378 *Current Science*, 34(9), 272–277.
- 379 Berry, D. I., & Kent, E. C. (2009). A new air-sea interaction gridded dataset from
 380 icoads with uncertainty estimates. *Bulletin of the American Meteorological So-*
 381 *ciety*, 90(5), 645–656.
- 382 Biasutti, M., Voigt, A., Boos, W. R., Braconnot, P., Hargreaves, J. C., Harrison,
 383 S. P., ... others (2018). Global energetics and local physics as drivers of past,
 384 present and future monsoons. *Nature Geoscience*, 11(6), 392–400.
- 385 Blanford, H. F. (1888). The rainfall of india. *Quarterly Journal of the Royal Me-
 386 teorological Society*, 14, 163–168.
- 387 Boos, W. R., & Korty, R. L. (2016, November). Regional energy budget control
 388 of the intertropical convergence zone and application to mid-holocene rain-
 389 fall. *Nature Geoscience*, 9(12), 892–897. Retrieved from <https://doi.org/10.1038/ngeo2833> doi: 10.1038/ngeo2833
- 390 Byrne, M. P., & Zanna, L. (2020, October). Radiative effects of clouds and water va-
 391 por on an axisymmetric monsoon. *Journal of Climate*, 33(20), 8789–8811. Re-
 392 trieved from <https://doi.org/10.1175/jcli-d-19-0974.1> doi: 10.1175/jcli-
 393 -d-19-0974.1
- 394 Ceppi, P., Brent, F., Zelinka, M. D., & Hartmann, D. L. (2017). Cloud feedback
 395 mechanisms and their representation in global climate models. *Wiley Interdis-
 396 ciplinary Reviews: Climate Change*, 8(4), e465.
- 397 Ceppi, P., & Hartmann, D. L. (2016). Clouds and the atmospheric circulation re-
 398 sponse to warming. *Journal of Climate*, 29(2), 783–799.
- 399 Chen, P.-J., Chen, W.-T., Wu, C.-M., & Yo, T.-S. (2021). Convective cloud regimes
 400 from a classification of object-based cloudsat observations over asian-australian
 401 monsoon areas. *Geophysical Research Letters*, 48(10), e2021GL092733.
- 402 Chen, W.-T., Wu, C.-M., & Ma, H.-Y. (2019). Evaluating the bias of south china
 403 sea summer monsoon precipitation associated with fast physical processes
 404 using a climate model hindcast approach. *Journal of Climate*, 32(14), 4491–
 405 4507.
- 406 Chepfer, H., Bony, S., Winker, D., Cesana, G., Dufresne, J., Minnis, P., ... Zeng, S.
 407 (2010). The gcm-oriented calipso cloud product (calipso-goccp). *Journal of
 408 Geophysical Research: Atmospheres*, 115(D4).
- 409 Chou, C., & Neelin, J. D. (2003). Mechanisms limiting the northward extent of
 410 the northern summer monsoons over north america, asia, and africa. *Journal
 411 of climate*, 16(3), 406–425.
- 412 Chou, C., Neelin, J. D., & Su, H. (2001). Ocean-atmosphere-land feedbacks in an
 413 idealized monsoon. *Quarterly Journal of the Royal Meteorological Society*,
 414 127(576), 1869–1891.
- 415 Clayson, C. A., Brown, J., & NOAA CDR Program. (2016). *Noaa climate data
 416 record (cdr) of ocean heat fluxes, version 2*. NOAA National Center for En-
 417 vironmental Information. Retrieved from <https://data.nodc.noaa.gov/cgi-bin/iso?id=gov.noaa.ncdc:C00973> (Ocean Heat Fluxes; SeaFlux OSB
 418 CDR: Heat Fluxes) doi: 10.7289/V59K4885
- 419 Dee, D. P., Uppala, S. M., Simmons, A., Berrisford, P., Poli, P., Kobayashi, S., ...
 420 others (2011). The era-interim reanalysis: Configuration and performance of
 421 the data assimilation system. *Quarterly Journal of the royal meteorological
 422 society*, 137(656), 553–597.
- 423 Donohoe, A., Marshall, J., Ferreira, D., & McGee, D. (2013). The relationship
 424 between itcz location and cross-equatorial atmospheric heat transport: From
 425 the seasonal cycle to the last glacial maximum. *Journal of Climate*, 26(11),
 426 3597–3618.
- 427 Gelaro, R., McCarty, W., Suárez, M. J., Todling, R., Molod, A., Takacs, L., ...
 428 others (2017). The modern-era retrospective analysis for research and applica-

- tions, version 2 (merra-2). *Journal of climate*, 30(14), 5419–5454.
- Gill, A. E. (1980). Some simple solutions for heat-induced tropical circulation. *Quarterly Journal of the Royal Meteorological Society*, 106(449), 447–462.
- Hamada, A., Murayama, Y., & Takayabu, Y. N. (2014). Regional characteristics of extreme rainfall extracted from trmm pr measurements. *Journal of Climate*, 27(21), 8151–8169.
- Hansen, J., Lacis, A., Rind, D., Russell, G., Stone, P., Fung, I., ... Lerner, J. (1984). Climate sensitivity: Analysis of feedback mechanisms. *feedback*, 1, 1–3.
- Harrop, B. E., & Hartmann, D. L. (2016, April). The role of cloud radiative heating in determining the location of the ITCZ in aquaplanet simulations. *Journal of Climate*, 29(8), 2741–2763. Retrieved from <https://doi.org/10.1175/jcli-d-15-0521.1> doi: 10.1175/jcli-d-15-0521.1
- Hersbach, H., Bell, B., Berrisford, P., Hirahara, S., Horányi, A., Muñoz-Sabater, J., ... Thépaut, J.-N. (2020). The era5 global reanalysis. *Quarterly Journal of the Royal Meteorological Society*, 146(730), 1999–2049. Retrieved from <https://rmets.onlinelibrary.wiley.com/doi/abs/10.1002/qj.3803> doi: <https://doi.org/10.1002/qj.3803>
- Hoskins, B. J., & Rodwell, M. J. (1995). A model of the asian summer monsoon. part i: The global scale. *Journal of Atmospheric Sciences*, 52(9), 1329–1340.
- Kanamitsu, M., Ebisuzaki, W., Woollen, J., Yang, S.-K., Hnilo, J., Fiorino, M., & Potter, G. (2002). Ncep–doe amip-ii reanalysis (r-2). *Bulletin of the American Meteorological Society*, 83(11), 1631–1644.
- Kang, S. M., Held, I. M., Frierson, D. M., & Zhao, M. (2008). The response of the itcz to extratropical thermal forcing: Idealized slab-ocean experiments with a gcm. *Journal of Climate*, 21(14), 3521–3532.
- Kobayashi, S., Ota, Y., Harada, Y., Ebita, A., Moriya, M., Onoda, H., ... others (2015). The jra-55 reanalysis: General specifications and basic characteristics. *Journal of the Meteorological Society of Japan. Ser. II*, 93(1), 5–48.
- Laguë, M. M., Swann, A. L., & Boos, W. R. (2021, 8). Radiative feedbacks on land surface change and associated tropical precipitation shifts. *Journal of Climate*, 34, 6651–6672. Retrieved from <https://journals.ametsoc.org/view/journals/clim/34/16/JCLI-D-20-0883.1.xml> doi: 10.1175/JCLI-D-20-0883.1
- Li, J., Wang, W. C., Dong, X., & Mao, J. (2017, 11). Cloud-radiation-precipitation associations over the asian monsoon region: an observational analysis. *Climate Dynamics*, 49, 3237–3255. Retrieved from <https://link.springer.com/article/10.1007/s00382-016-3509-5> doi: 10.1007/S00382-016-3509-5/FIGURES/13
- Li, Y., Thompson, D. W., & Bony, S. (2015). The influence of atmospheric cloud radiative effects on the large-scale atmospheric circulation. *Journal of Climate*, 28(18), 7263–7278.
- Loeb, N. G., Doelling, D. R., Wang, H., Su, W., Nguyen, C., Corbett, J. G., ... Kato, S. (2018). Clouds and the earth's radiant energy system (ceres) energy balanced and filled (ebaf) top-of-atmosphere (toa) edition-4.0 data product. *Journal of Climate*, 31(2), 895–918.
- Lu, J., Xue, D., Leung, L. R., Liu, F., Song, F., Harrop, B., & Zhou, W. (2021). The leading modes of asian summer monsoon variability as pulses of atmospheric energy flow. *Geophysical Research Letters*, 48. doi: 10.1029/2020GL091629
- Luo, Z. J., Anderson, R. C., Rossow, W. B., & Takahashi, H. (2017). Tropical cloud and precipitation regimes as seen from near-simultaneous trmm, cloudsat, and calipso observations and comparison with isccp. *Journal of Geophysical Research: Atmospheres*, 122(11), 5988–6003.
- Ma, H.-Y., Xie, S., Klein, S., Williams, K., Boyle, J., Bony, S., ... others (2014). On the correspondence between mean forecast errors and climate errors in cmip5

- models. *Journal of Climate*, 27(4), 1781–1798.
- Neelin, J. D. (2007). Moist dynamics of tropical convection zones in monsoons, teleconnections, and global warming. *The global circulation of the atmosphere*, 267, 301.
- Peterson, H. G., & Boos, W. R. (2020, 3). Feedbacks and eddy diffusivity in an energy balance model of tropical rainfall shifts. *npj Climate and Atmospheric Science* 2020 3:1, 3, 1-9. Retrieved from <https://www.nature.com/articles/s41612-020-0114-4> doi: 10.1038/s41612-020-0114-4
- Plumb, R. A. (2007). Dynamical constraints on monsoon circulations. *The Global Circulation of the Atmosphere*, 252, 266.
- Popp, M., & Silvers, L. G. (2017). Double and single itczs with and without clouds. *Journal of Climate*, 30(22), 9147–9166.
- Privé, N. C., & Plumb, R. A. (2007). Monsoon dynamics with interactive forcing. part ii: Impact of eddies and asymmetric geometries. *Journal of the atmospheric sciences*, 64(5), 1431–1442.
- Rajeevan, M., & Srinivasan, J. (2000, February). Net cloud radiative forcing at the top of the atmosphere in the asian monsoon region. *Journal of Climate*, 13(3), 650–657. Retrieved from [https://doi.org/10.1175/1520-0442\(2000\)013<0650:ncrfat>2.0.co;2](https://doi.org/10.1175/1520-0442(2000)013<0650:ncrfat>2.0.co;2) doi: 10.1175/1520-0442(2000)013<0650:ncrfat>2.0.co;2
- Randall, D. A., Dazlich, D. A., & Corsetti, T. G. (1989). Interactions among radiation, convection, and large-scale dynamics in a general circulation model. *Journal of Atmospheric Sciences*, 46(13), 1943–1970.
- Saha, S., Moorthi, S., Wu, X., Wang, J., Nadiga, S., Tripp, P., ... others (2014). The ncep climate forecast system version 2. *Journal of climate*, 27(6), 2185–2208.
- Saud, T., Dey, S., Das, S., & Dutta, S. (2016, 12). A satellite-based 13-year climatology of net cloud radiative forcing over the indian monsoon region. *Atmospheric Research*, 182, 76-86. doi: 10.1016/J.ATMOSRES.2016.07.017
- Sharma, O. P. (1998). Interannual variations of summer monsoons: Sensitivity to cloud radiative forcing. *Journal of Climate*, 11. doi: 10.1175/1520-0442-11.8.1883
- Shekhar, R., & Boos, W. R. (2016). Improving energy-based estimates of monsoon location in the presence of proximal deserts. *Journal of Climate*, 29(13), 4741–4761.
- Sherwood, S. C., Ramanathan, V., Barnett, T. P., Tyree, M. K., & Roeckner, E. (1994). Response of an atmospheric general circulation model to radiative forcing of tropical clouds. *Journal of Geophysical Research: Atmospheres*, 99(D10), 20829–20845.
- Slingo, A., & Slingo, J. (1988). The response of a general circulation model to cloud longwave radiative forcing. i: Introduction and initial experiments. *Quarterly Journal of the Royal Meteorological Society*, 114(482), 1027–1062.
- Sohn, B.-J., & Smith, E. A. (1992). Global energy transports and the influence of clouds on transport requirements—a satellite analysis. *Journal of climate*, 5(7), 717–734.
- Sperber, K., Annamalai, H., Kang, I.-S., Kitoh, A., Moise, A., Turner, A., ... Zhou, T. (2013). The asian summer monsoon: an intercomparison of cmip5 vs. cmip3 simulations of the late 20th century. *Climate dynamics*, 41(9), 2711–2744.
- Stevens, B., Bony, S., & Webb, M. (2012). *Clouds on-off klimate intercomparison experiment (cookie)*.
- Su, H., & Neelin, J. D. (2002). Teleconnection mechanisms for tropical pacific descent anomalies during el niño. *Journal of the Atmospheric Sciences*, 59. doi: 10.1175/1520-0469(2002)059<2694:TMFTPD>2.0.CO;2
- Tian, B., & Ramanathan, V. (2002). Role of tropical clouds in surface and atmospheric energy budget. *Journal of climate*, 15(3), 296–305.

- 541 Voigt, A., & Albern, N. (2019). No cookie for climate change. *Geophysical Research
Letters*, 46(24), 14751–14761.
- 542 Voigt, A., Bony, S., Dufresne, J.-L., & Stevens, B. (2014, June). The radiative
543 impact of clouds on the shift of the intertropical convergence zone. *Geophys-
ical Research Letters*, 41(12), 4308–4315. Retrieved from <https://doi.org/10.1002/2014gl060354> doi: 10.1002/2014gl060354
- 544 Voigt, A., & Shaw, T. A. (2015, January). Circulation response to warming
545 shaped by radiative changes of clouds and water vapour. *Nature Geoscience*,
546 8(2), 102–106. Retrieved from <https://doi.org/10.1038/ngeo2345> doi:
547 10.1038/ngeo2345
- 548 Xie, S., Ma, H.-Y., Boyle, J. S., Klein, S. A., & Zhang, Y. (2012). On the correspon-
549 dence between short-and long-time-scale systematic errors in cam4/cam5 for
550 the year of tropical convection. *Journal of Climate*, 25(22), 7937–7955.
- 551 Xie, S.-P., Tanimoto, Y., Noguchi, H., & Matsuno, T. (1999). How and why cli-
552 mate variability differs between the tropical atlantic and pacific. *Geophysical
Research Letters*, 26(11), 1609–1612.
- 553 Yu, L., & Weller, R. A. (2007). Objectively analyzed air-sea heat fluxes for the
554 global ice-free oceans (1981–2005). *Bulletin of the American Meteorological So-
ciety*, 88(4), 527–540.
- 555 Yuan, J., & Houze, R. A. (2010). Global variability of mesoscale convective system
556 anvil structure from a-train satellite data. *Journal of Climate*, 23(21), 5864–
557 5888.
- 558 Zeng, N., & Neelin, J. D. (1999). A land-atmosphere interaction theory for the
559 tropical deforestation problem. *Journal of Climate*, 12. doi: 10.1175/1520-
560 -0442(1999)012<0857:alaitf>2.0.co;2
- 561
- 562
- 563
- 564
- 565

Supporting Information for “The Unexpected Oceanic Peak in Energy Input to the Atmosphere and its Consequences for Monsoon Rainfall”

Nandini Ramesh^{1,2}, William R. Boos^{2,3}

¹ARC Centre for Data Analytics for Resources and the Environment, University of Sydney, 1 Cleveland Street, Darlington 2008, NSW, Australia.

²Department of Earth and Planetary Science, University of California, Berkeley, McCone Hall, Berkeley, California, 94720

³Climate and Ecosystem Sciences Division, Lawrence Berkeley National Laboratory, 1 Cyclotron Road, Berkeley, CA 94720

Contents of this file

1. Figures S1 to S3

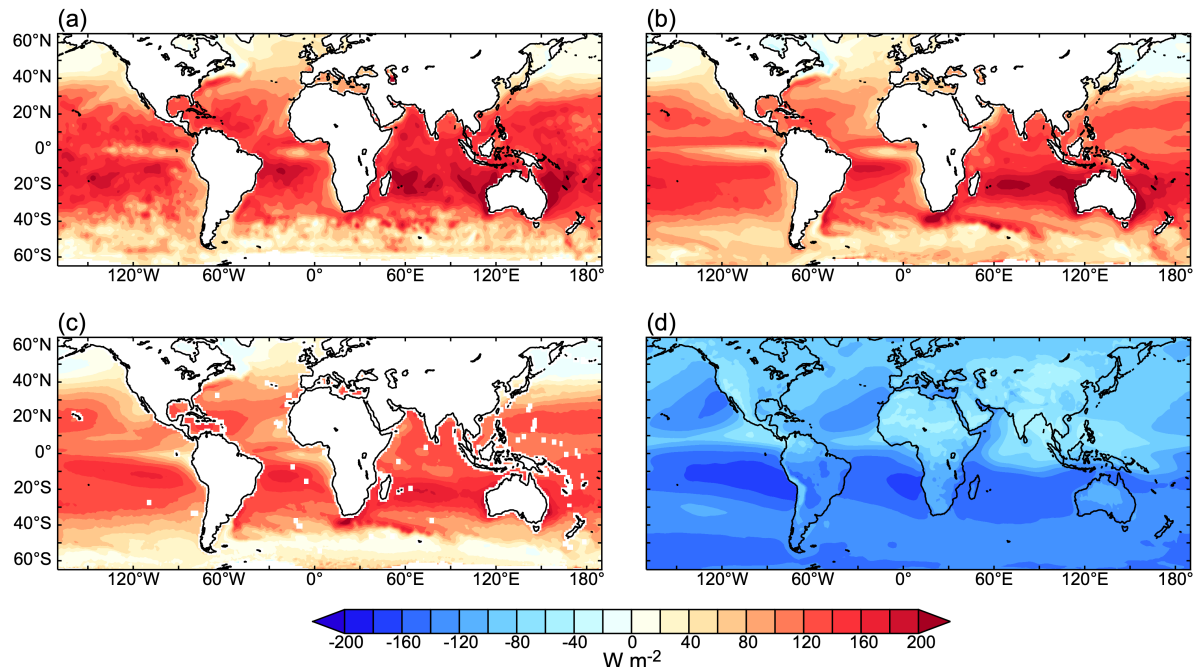


Figure S1. Climatological turbulent air-sea fluxes into the atmosphere during June-August from various data sources (a-c) and net radiative flux convergence from CERES vertically integrated over the atmosphere (d): (a) NOCS, (b) OAFlux, (c) SeaFlux. Positive values indicate a flux into the atmospheric column.

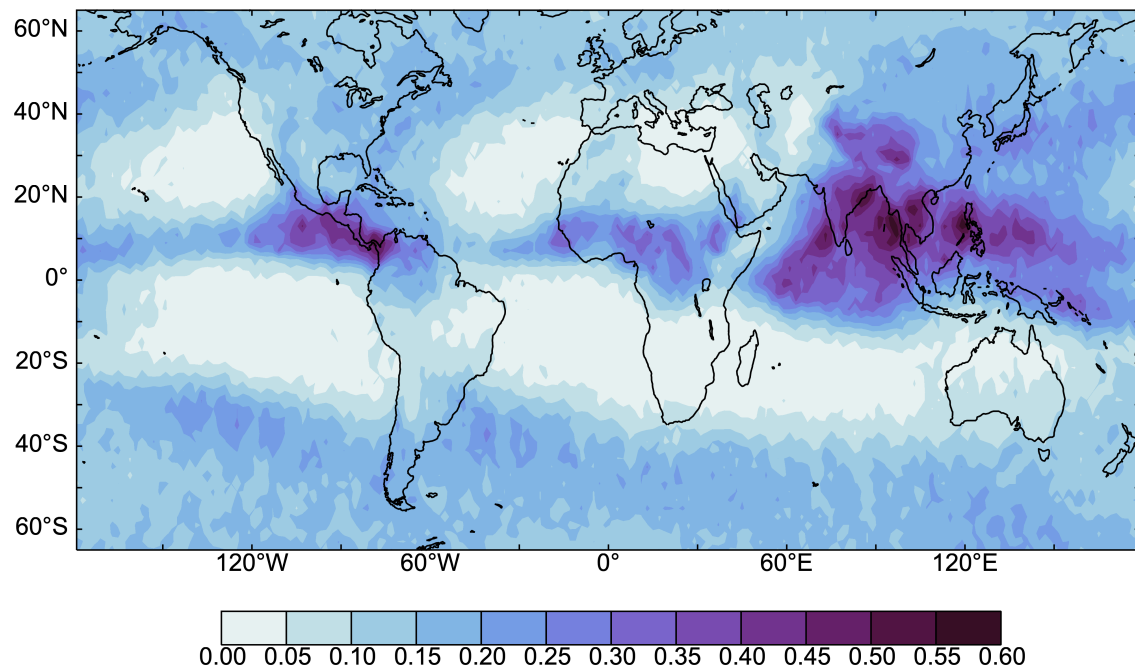


Figure S2. The climatological high cloud fraction during June-August from CALIPSO-GOCCP. Note the large high cloud fraction over the South Asian region and in particular, the Bay of Bengal.

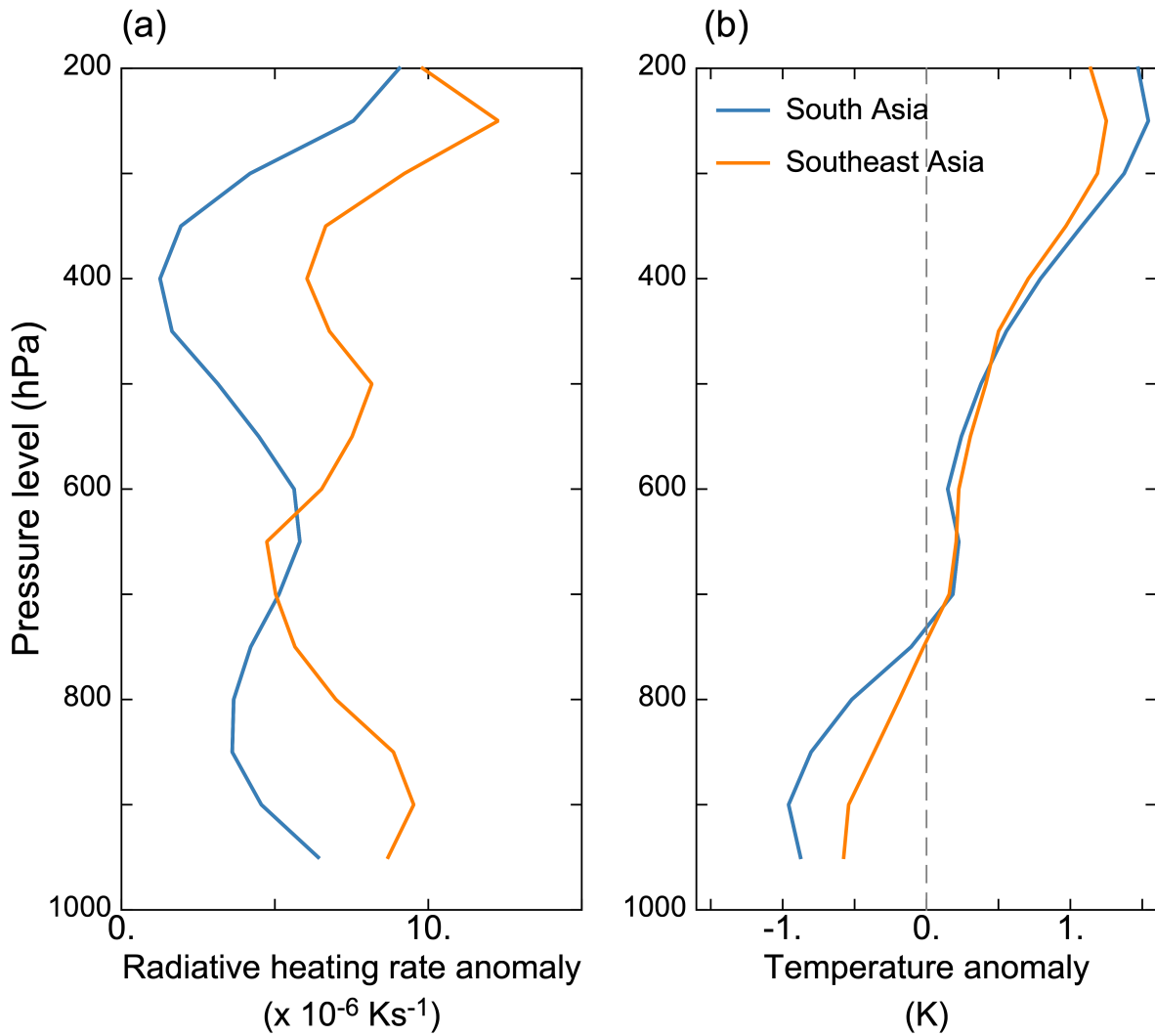


Figure S3. The anomaly (control minus noTropicCloud) in (a) radiative heating rate and (b) temperature averaged over South (70°E-90°E, 10°N-30°N) and Southeast (90°E-110°E, 10°N-30°N) Asia. The net effect of CRE on the tropospheric radiative heating in both locations is positive, and is accompanied by a large, $O(100 \text{ W m}^{-2})$, reduction in surface fluxes of sensible and latent heat; these effects together produce the convective stabilization of the atmosphere seen in the anomalous temperature profiles in (b).